Recent Developments in Ultraorientation of Polyethylene by Solid State Extrusion

ANAGNOSTIS E. ZACHARIADES, W. T. MEAD, and ROGER S. PORTER*

Polymer Science and Engineering Department, Materials Research Laboratory, University of Massachusetts, Amherst, Massachusetts 01003

Received June 15, 1979 (Revised Manuscript Received June 30, 1980)

Contents

I. Introduction

Polymers in the bulk are generally composed of long molecular chains in which the monomers are covalently bonded along the chain direction. Such covalent bonding of carbon atoms is responsible for the high strength of diamond, nature's strongest material. However, manmade polymers do not exhibit the corresponding potential high modulus. High modulus and strength, as now known, may result from a structure of straight, stable, and densely packed chains.

Polymer chains normally are not stretched out, but they assume a configuration which lacks overall orientation and has chain folds at the edges of polymer crystals when semicrystalline polymers are in this isotropic state. Their crystallites lack the stretched chains on which tensile strength depends. The aim therefore is to eliminate chain folding and to align, orient, and closely pack the macromolecular chains into a rigid-chain configuration for the pursuit of high modulus polymers.

Polymer researchers have approached the problem of making the strongest possible polymers in two diverse ways: (1) by chemically constructing polymers with rigid and linear backbone chains and (2) by processing existing conventional polymers in ways that a permanent transformation of the internal structure and properties occurs. Chemical construction of rigid macromolecules has been approached by syntheses leading to para-substituted aromatic rings in the polymer backbone. In general, these polymers cannot be processed by means of the common polymer-processing techniques; however, some industrial examples, viz, Kevlar and X-500, have been processed into fibers (of very high strength).

In the second category, polymers are converted into a highly oriented chain configuration with substantially increased modulus by drawing from a dilute flowing solution, or by extruding a supercooled melt, or by solid-state extruding or drawing below the melting point under controlled conditions.

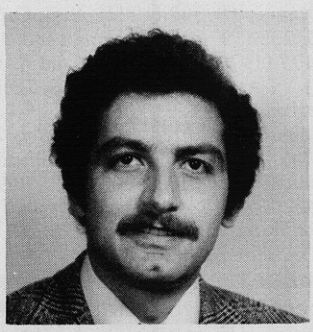

Anagnostis E. Zachariades was born in Greece and received his B.Sc. in Chemistry from The University of Aston in Birmingham (England) and his Ph.D. in Polymer Chemistry from SUNY College of Environmental Science and Forestry in Syracuse, NY. After his Ph.D he joined the University of Massachusetts as research associate for 3 years. Presently, he is a research staff member at the IBM Research Division in San Jose, CA. His interests are centered on the morphology, mechanical properties, and the process–structure–property relationships of polymers.

W. T. Mead obtained his B.Sc. (honors) in physics at Nottingham University and a Ph.D. in materials science at University of London. He did postdoctoral work with Professors Roger S. Porter and Richard S. Stein at University of Massachusetts. After working at Goodyear in Europe and Dow Chemical of Canada, he jointed the staff of Dow Chemical USA, Central Research Plastics Laboratory.

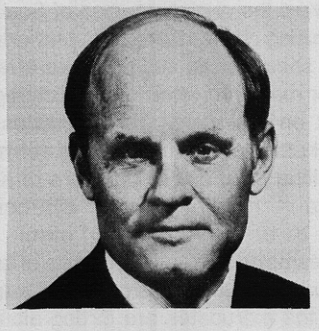

Roger S. Porter is Co-Director of the Materials Research Laboratory, University of Massachusetts. He was born in 1928 in Windom, MN, and received degrees from University of California, Los Angeles (B.S., Chemistry, 1950) and University of Washington (Ph.D., Chemistry, 1956). He has previously been visiting professor at Royal Institute of Technology, Stockholm (1972) and University of London, Queen Mary College (1972–1973). At the University of Massachusetts he has been Associate Professor and Chairman (1966–1968), Professor and Department Head (1968–1976), and Professor (1976–) in Polymer Science and Engineering.

0009-2665/80/0780-0351$05.00/0

TABLE I. Presently Achievable Tensile Properties of Materials

material	tensile modulus, GPa: small crystals	tensile modulus, GPa: bulk samples	tensile strength, GPa
polypropylene	42[a]	22[b]	0.93[b]
polyethylene	240[a]	70[c]	0.60[e]
polystyrene	12[a]	4-5[d]	0.08[d]
carbon steel SAE 1020	208[f]		0.45-0.62[f]
aluminum	69[f]		0.09-0.17[f]
glass fiber	69-183[g]		0.39-0.69[f]

[a] I. Sakurada, T. Ito, and K. Nakamae, *J. Polym. Sci.*, 15, 75 (1966). [b] W. N. Taylor and E. S. Clark, *Polym. Prep., Am. Chem. Soc., Div. Polym. Chem.*, 18, 332 (1977). [c] G. Capaccio and I. M. Ward, *Polymer*, 15, 233 (1974); N. J. Capiati and R. S. Porter, *J. Polym. Sci.*, 13, 1177 (1975); P. J. Barham and A. Keller, *J. Mater. Sci.*, 11, 27 (1976). [d] A. E. Zachariades, E. S. Sherman, and R. S. Porter, *J. Appl. Polym. Sci.*, 24, 2137 (1979). [e] T. Kanamoto, A. E. Zachariades, and R. S. Porter, *J. Polym. Sci., Polym. Phys. Ed.*, 17, 2171 (1979). [f] J. H. Perry, "Chemical and Engineering Handbook", 4th ed., McGraw-Hill, New York, 1969, Section 23, p 31. [g] N. J. Parrat, "Fiber Reinforced Materials Technology", Van Nostrand, New York, 1972, p 68.

Solid-state extrusion has been an area in which considerable knowledge has been gained recently. In this article we review this process in structural and morphological terms and discuss the effect of deformation (processing) conditions on the physical and mechanical properties. Studies were initiated with the deformation of high-density polyethylene through tapered dies[1-3] using an Instron capillary rheometer; more conventionally, this instrument is used to evaluate the flow properties of liquid or semiliquid materials, including molten polymers, elastomeric compounds, and other materials. The lower part of the rheometer is fitted with a die of conical or wedge-shape geometry through which the material is extruded. In ram or direct extrusion the polymer is deformed under the direct plunger force of the extruder whereas in hydrostatic extrusion the pressure is exerted through a surrounding pressure transmitting fluid (e.g., castor oil). Polyethylene extrudates were produced by crystallizing the polymer melt under the combined orientation and pressure effects in an Instron capillary rheometer under controlled processing conditions. The polymer crystallized in the conical entrance of the die and in the rheometer barrel. The semicrystalline mass was then forced at constant velocity into the relatively narrow diameter capillary section of the die at pressures resulting in intense shear stress. In their original experiments, Southern and Porter[1] reported that pressure rapidly increased after crystallization had occurred, and extrusion at constant velocity could not be maintained. This technique was subsequently modified by Capiati et al.[4] by preparing the polymer crystal morphology in situ prior to solid-state extrusion. The method differs from the original method of Southern and Porter in the way of inducing crystallization; i.e., previously crystallization was induced by shear stress and pressure effects on the melt while in the latter method crystallization occurred under only the pressure effect on the melt. This produces an equilibrium spherulitic morphology at an undercooling corresponding to the elevation of melting point due to pressure of about 20 °C per 0.1 GPa[5] (1 GPa = 10^9 N/m^2 = 10^{10} dyn/cm^2 = 1.1 × 10^4 kg/cm^2 = 1.45 × 10^5 psi = 0.99 10^4 atm).

The extruded samples have a high degree of crystal orientation in combination with the unusual property of transmitting visible light. Although the extrudates are strong along the extrusion direction, i.e., possess high tensile modulus, the radial strength is limited to weak van der Waals forces and therefore extrudates easily split when they are deformed or compressed along the radius.[6]

The production of ultraoriented fibers of more perfect structure with a tensile modulus approaching the theoretical value (see Table I) necessitated the evaluation of the relationships between extrusion variables and the consequent fiber properties. Imada et al.[7-9] have studied the hydrostatic extrusion of high-density polyethylene and other semicrystalline polymers. A related investigation was undertaken in this laboratory.[10,11] However, the characteristics of the hydrostatic extrustion and of the conventional ram method have not been compared, nor have the corresponding physical properties of the extrudates been evaluated. According to Alexander,[12] only hydrostatic extrusion has the potential of being a continuous process because of the reduced friction between the polymer and the die wall and the decrease in strain hardening. However, this limitation now has been alleviated to a large extent by the two new techniques of solid-state coextrusion and coextrusion aided by drawing.[13,14] These two method produce steady-state extrusion at high extrusion draw ratios and at unusually fast extrusion rates under moderate processing conditions without lubricant aids. The solid-state coextrusion method briefly involves the introduction of longitudinal free surface areas in preformed crystalline morphologies. These effectively change and relieve the stresses which normally develop during a conventional extrusion.

II. Deformation Mechanisms and Structural Models

Polyethylene has been considered a prime candidate for deformation studies in this and other laboratories for various reasons. The polymer has no pendant groups, is linear, and has a small cross-sectional crystal area (18 Å^2/chain). In addition, its semicrystalline nature allows storing of energy within the polymer in such a way that elongation and orientation of the polymer chains can occur while the whole sample is deformed. However, in order to orient, elongate, align, and pack the individual chains at the highest concentration per sectional area, one must examine what happens to the initial isotropic, spherulitic structure during deformation.

A spherulite may be envisaged as an isolated structure consisting of folded-chain lamellae arranged radially about its center. The spherulites surrounded by the amorphous phase are connected to other spherulites through intercrystalline chain molecules called tie molecules.[15,16] Upon deformation, the spherulites change from a spherical to an ellipsoidal shape as shown in Figure 1. At higher deformation, however, the lamellar deformation will depend on the orientation of the lamellae with respect to the stretch direction. Characteristically, lamellae aligned parallel to the stretch direction disrupt in the center of the spherulite, those oriented at angles from 30° to 60° to the stretch direction undergo lamellar slip, while lamellae aligned along the equatorial direction of the spherulite undergo further separation. Thus as the spherulites deform, lamellae reorient themselves along the stress direction and at yield stress, when necking occurs, the spherulitic structure is converted to a fibrillar structure.[15]

A detailed review on spherulitic deformation using high-density polyethylene has been reported by Hay and Keller.[17] Upon drawing, they notice two types of spherulitic deformation: (1) homogeneous and (2) inhomogeneous. In the first, all parts of a given spherulite extend simultaneously and proportionally. In the latter, the spherulites and/or regions between them yield in areas that draw out fully. Further extension occurs by the drawn-out regions spreading at the expense of unyielded regions. In addition, these authors report that often the deformation within a spherulite is greater than that in the material between spherulites, indicating a weakness within the spherulites.

Other authors[18-22] have studied also the spherulite deformation of polyethylene. Stein, working mainly with low-density polyethylene, has found[23] that although the overall spherulite length may vary in proportion with the sample dimensions upon stretching, the microstructure may not. Often the spherulite is

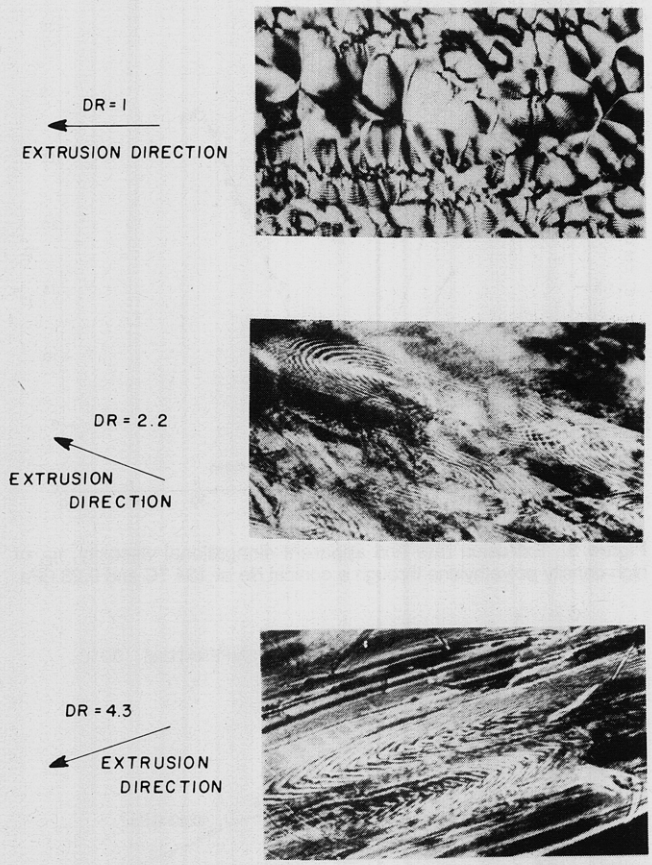

Figure 1. Morphological transformation of high-density polyethylene during solid state extrusion. (Photographs kindly provided by Dr. F. Khoury, National Bureau of Standards, Washington, DC).

found to deform predominantly near the equator.[17,24] Such a process depends on the rate of deformation and may lead to density depletion in the equatorial region, probably associated with the formation of microvoids between separating lamellae. Thus if a polymer is stretched at a high strain rate, large stresses and hence strains will concentrate on intercrystalline tie chains as the crystal orientation will lag behind the strain and therefore make the polymer brittle. Alternatively, if the strain rate is slow, deformation will be more uniform over the sample. The rate of structural response and the resulting mechanical properties depend upon the size, perfection, and organization of the crystalline and amorphous regions.[23]

A high degree of crystal orientation is not the only factor associated with high tensile modulus.[25] Peterlin[26-28] and others[29,30] propose that the strongest element of the oriented polymer is the microfibril. The microfibril consists of highly oriented folded-chain molecules connected by many tie molecules within the amorphous phase separating the lamellae (Figure 2). These authors attribute the increase in fiber strength with draw ratio to the increase in the number of tie molecules that arises from chain unfolding when lamellar blocks slip past each other during necking. Porter[31] introduced the concept of "the continuous crystal" to relate the effects of morphological changes to tensile properties. The concept corresponds to a crystal model composed of perfectly oriented extended-chain molecules with the chain ends randomly located in the crystal.

Table I provides a comparison of experimental and theoretical tensile moduli for polymers and other materials. It is noted that the tensile modulus of the ultradrawn polyethylene is still one order of magnitude below its ultimate strength although the molecules have been oriented. This is due to a significant number of chain folds in the lamellae and a limited number of tie molecules between them. The modulus may increase either by increasing the number of tie molecules as mentioned above

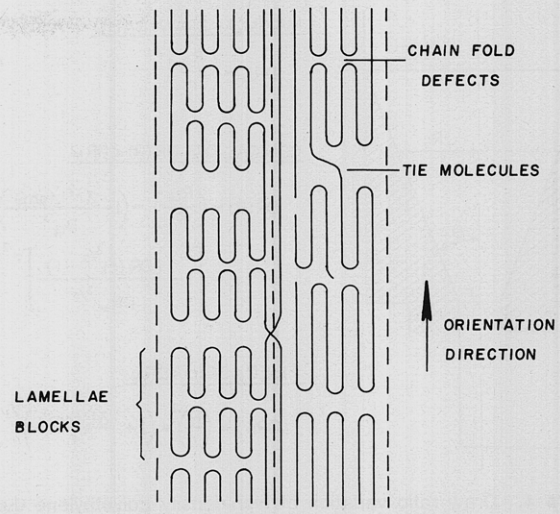

Figure 2. Schematic structure of drawn crystalline polymer (after Peterlin[26]).

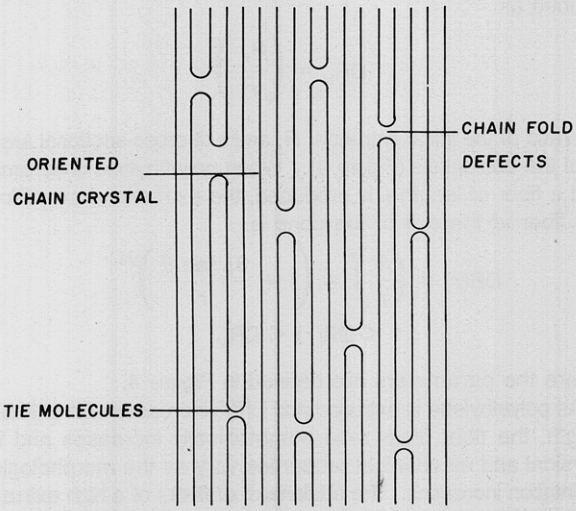

Figure 3. Schematic representation of extended chain-lamellar block crystal structure (after Clark and Scott[35]).

or by reducing the number of chain folds. The number of tie molecules increases by drawing the material beyond its natural draw ratio, a material property sensitive to temperature, molecular weight, and drawing rate conditions.[32] Fully extended chain molecules can be formed only when the draw ratio exceeds the ratio for the random-coil to extended-chain dimension.[33] For polyethylene, the minimum ratio required to fully extend the chain varies from 8.6 for average molecular weight $M_w = 10^4$ to 86 for $M_w = 10^6$ and becomes even higher for higher molecular weight materials.[33] However, completely extended chains may not be required for maximum strength as the polymer will fail upon shearing. Frank[34] reports the optimum strength is obtained when only 50% of the molecules are fully extended. Chain-extended morphologies have been prepared by crystallization under high pressure,[6] the superdrawing method[35] devised by Clark and Scott, and the solid-state extrusion process. Figure 3 shows a schematic proposed by Clark and Scott for a model describing these chain-extended morphologies.

III. Extrusion Variables

Extrusion variables which significantly affect the rate of extrusion are draw ratio, extrusion temperature and pressure, angle of the conical die, and lubricant aids (the term extrusion draw ratio is used in the text when referring to solid-state extrusion). In the work reported in the present article no lubricating aids were used and the conical dies had a 20° cone angle.

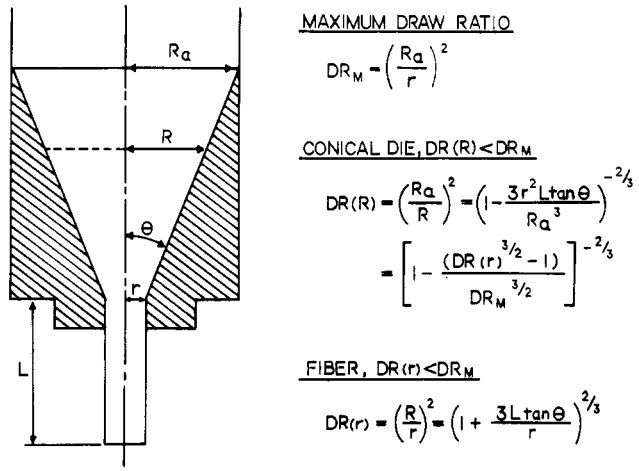

Figure 4. Draw ratio variation of high-density polyethylene during solid-state extrusion through a conical die.

The maximum draw ratio, $(DR)_M$, of the extruded material is defined as

$$DR_M = \left(\frac{R_a}{r}\right)^2 \tag{1}$$

the ratio of the initial entrance, R, and exit cross-sectional areas, r, of the conical die (Figure 4). When polyethylene is deformed and a fiber of length L is produced, the extrusion draw ratio of the fiber at the exit of the cone is

$$DR(r) = \left(\frac{R}{r}\right)^2 = \left(1 + \frac{3L\tan\theta}{r}\right)^{2/3} \tag{2}$$
$$1 < DR(r) < DR_M$$

where the parameters are defined in Figure 4.

As polyethylene is extruded and $DR(r)$ increases with extrusion length, the fiber draw ratio monotonically increases and the physical and mechanical properties vary as the morphological orientation increases. The attainment of fibers of a high extrusion draw ratio is one of the most important aspects of solid-state extrusion for production of high modulus fibers.

The relationship between extrusion rate dL/dt and time t to attain a given draw ratio can be deduced for the initial condition by using the equation of continuity for polymer flow through a conical die. The relationship given by Snelling and Lontz[36] is

$$t = \frac{k}{\frac{dL}{dt}}[DR^{3/2} - 1] \tag{3}$$

for $DR(r) < DR_M$; $k = 2r(1 - \cos\theta)/(3\sin^2\theta)$, $\theta = 20°$, $r = 0.066$ cm. With increasing draw ratio, extrusion rate approaches a constant value depending on the extrusion variables.

Extrusion rate data in terms of an apparent elongational viscosity are shown in Figure 5 for HDPE extruded at 134 °C. The viscosity is defined as[37]

$$\eta_E = \frac{\sigma_z}{\gamma_E} \tag{4}$$

where σ_z is the axial stress assumed to be equal to the constant applied pressure, γ_E is the elongation rate, $\gamma_E = (1/L)\,dL/dt$, and L is the extrusion length. The rate rapidly decreases with increasing draw ratio and approaches a constant value. The corresponding curve for η_E shows that the apparent elongation viscosity is weakly dependent on draw ratios below 15. This is because deformation of the original spherulitic polyethylene in the die can proceed at high rates, producing low nucleation. After fibrillar morphology is formed near the tip of the conical billet, strain hardening follows, as shown by the increase of η_E

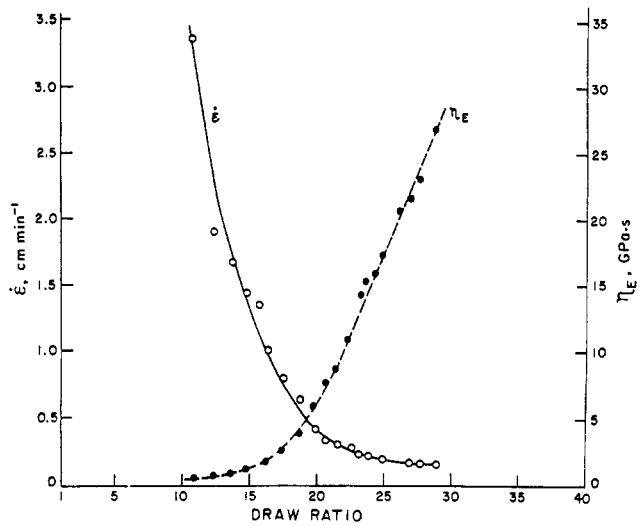

Figure 5. Extrusion rate and apparent elongational viscosity, η_E, of high-density polyethylene through a conical die at 134 °C and 0.23 GPa.

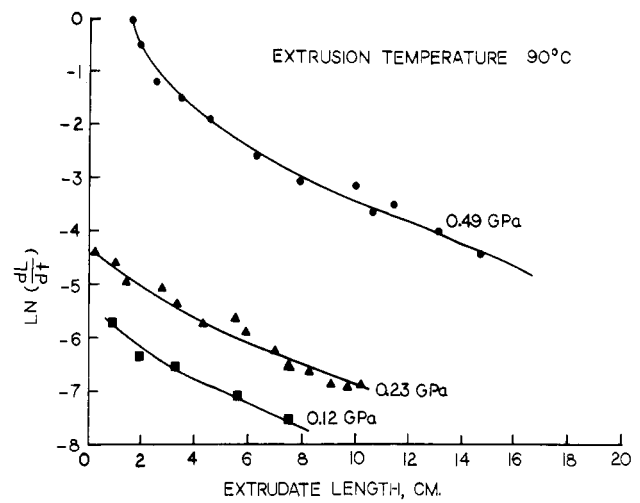

Figure 6. Logarithm of extrusion rate vs. fiber length L at 90 °C and at pressures 0.23–0.49 GPa.

with draw ratio.

Figure 6 shows the logarithm of extrusion rate as a function of extrudate length for fibers extruded at constant applied pressures from 0.12 to 0.49 GPa. The variation of the logarithm of the limiting flow rates with draw ratio is approximately proportional to the applied pressure. Increase of applied pressure will also increase the melting point and undercooling according to

$$\Delta T = T_M + 200P_c - T_E \tag{5}$$

where P_c is the applied extrusion pressure (expressed in GPa), T_E is the extrusion temperature, and T_M is the equilibrium melting point for a perfect polyethylene single crystal (145 ± 1 °C).[5] Since the extrusion rate and therefore η_E vary with pressure, the extrusion rate will be given by

$$\frac{dL}{dt} = c\int_{p=0}^{p=P}\frac{dp}{\eta_E(p)} \tag{6}$$

where c is a constant for a given die and the pressure at the die exit is assumed to be 1 atm, so the lower limit of the integral is set equal to zero since $P \gg 1$.

The pressure dependence of η_E may thus be obtained from the slope of extrusion rate with applied pressure P. Since η_E decreases with P as shown by the variation of ln $[(1/L)\,dL/dt]$ with pressure in Figure 7, then dL/dt will increase with P. A

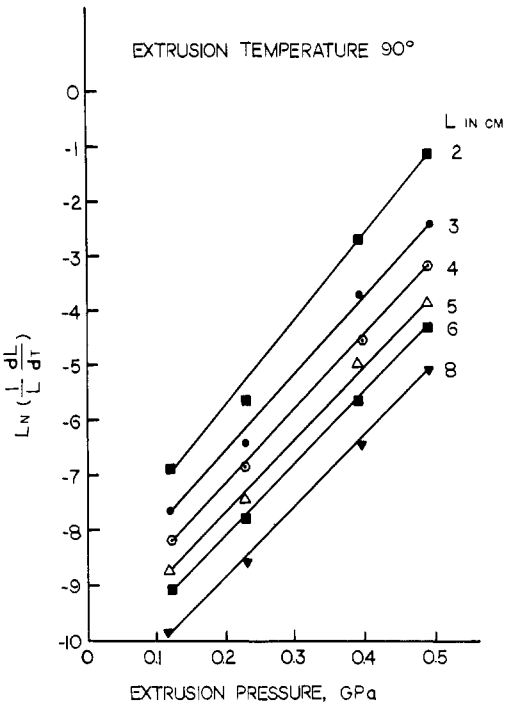

Figure 7. Variation of ln (dL/dt) with pressure for HDPE extruded at 90 °C.

simple empirical form of η_E which can be used to fit such data is

$$\eta_E = \eta_0 \exp(aP) \tag{7}$$

where a is constant and $(dL/dt)/P = A[1 - \exp(-aP)]$, where A is constant. The logarithmic dependence of extrusion rate on pressure, as shown in Figure 7, is in accord with the yield theory of Eyring[38] and appears to be applicable to solid-state extrusion under constant pressure in the temperature range 80–130 °C.[10,39]

The temperature dependence of extrusion rates can be explained in terms of stress-aided thermal activated processes.[40] Variation of the rate dependence of polyethylene flow with temperature and pressure, as measured by the apparent elongational viscosity η_E, or $(dL/dt)(1/L)$, will give information concerning the nature of the deformation, i.e.

$$\eta_E = \eta_0 \exp\left(\frac{E^*}{RT}\right) \tag{8}$$

where η_0 is a rate constant, E^* is an apparent activation energy for the deformation, which may vary with strain, and R is the gas constant. Activation energies are obtained from the slope of a plot of log η_E vs. $1/T$(K), given in Figure 8. Mead and Porter[10] report a break in the curve of extrusion rate vs. temperature for extruded high-density polyethylene and explain this anomaly as possibly due to an increase in friction between the die and the polymer and/or the change in the α relaxation with pressure. They also report that in the processing temperature range 80–100 °C, which corresponds to the temperature range of α relaxation for polyethylene, the maximum tensile properties were obtained. The reorganization of crystallites may be divided into two mechanisms (α_1 and α_2), inter- and intralamellar motions. The α_1 (grain boundary) relaxation mechanism is reported to arise from the deformation and rotation of elastic crystalline lamellae within the viscous medium.[41] The α_2 mechanisms arises from deformation of cyrstalline lamellae due to the onset of torsional oscillations of polymer chains within the crystal lattice. Mead and Porter[10] therefore suggest that the first stage of extrusion, as shown in Figure 5, related to the α_1 grain boundary mechanism. The lamellae are then further deformed according to the α_2 mechanism. It is during this second drawing stage that the highest physical and mechanical properties of the fibers will be attained. This is discussed further in the following section.

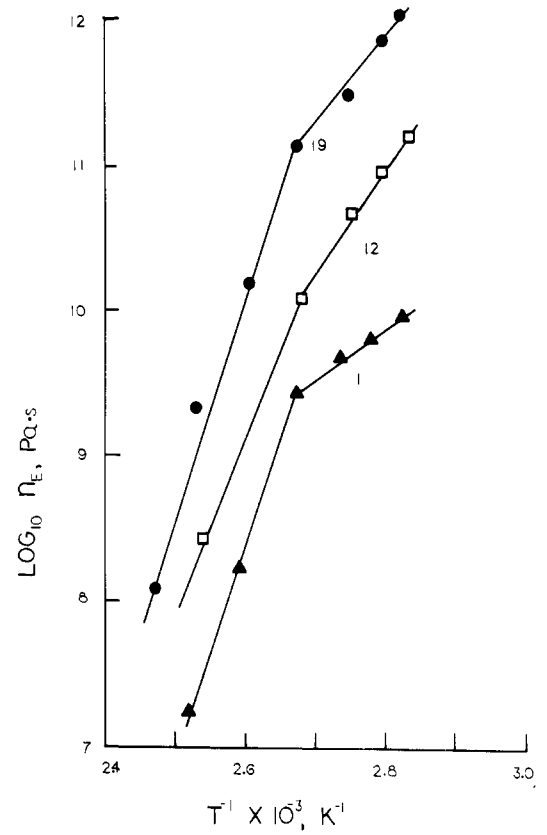

Figure 8. Plot of logarithm of η_E vs. $1/T$(K) of extrusion. Comparisons at fiber length L cm.

IV. Physical and Mechanical Properties

In a uniaxially drawn or extruded polymer, the distribution of the orientation of the crystallites may be described by an orientation distribution function, f(θ), where θ is the angle between the chain axis and the drawn direction. Ward has shown[42] that the distribution function may be expanded in a series of Legendre polynomials or orientational distribution coefficients, $\overline{P_n(\cos\theta)}$. The values of $\overline{P_n(\cos\theta)}$ may be determined by spectroscopic techniques.[43]

X-ray measurements of the orientation of the crystallographic c axis of the extruded fibers have been made to determine the second moment data, i.e., $\overline{P_2 \cos\theta} = {}^1/_2(3\overline{\cos^2\theta} - 1)$. The value may also be determined from birefringence measurements, Δn, since $\Delta n = \overline{P_2(\cos\theta)}\Delta n_c^\circ$, where Δn_c° is the maximum or intrinsic birefringence. Birefringence is the difference in refractive index parallel and perpendicular to the fiber axis and will vary with orientation of both crystalline and noncrystalline phases. The total second or fourth moment may each be written as the sum of the noncrystalline and crystalline contributions. Other spectroscopic techniques may be used to determine the second and fourth moment orientation functions, e.g., infrared, absorption dichroism, Raman, polarized fluorescence, and broad-line NMR. Miller et al.[44] determined the orientation functions of the extruded HDPE fibers by using IR spectroscopy. The broad-line NMR results for these fibers are discussed below.

The weight fraction of crystallinity and the melting point of the extruded fibers were assessed by differential scanning calorimetry. Thermal shrinkage of the fibers parallel to the fiber

axis was also measured, and the perfection of the fibers was assessed by comparing with the linear expansion coefficient of a single polyethylene crystal along the *c* crystallographic axis.

Small-angle X-ray analysis of the fibers has also been used to measure fiber perfection. The periodicity of lamellar stacking or long period, L, was calculated from the scattering maximum according to Bragg's law. No long period is observed for a perfectly oriented fiber, and hence the intensity of the first-order diffraction pattern gives information on the perfection of the extruded fiber.

Continuous fibers which have their crystalline unit cells perfectly aligned along the fiber length will have maximum mechanical properties. Calculated maximum longitudinal crystal moduli from force constants for linear HDPE are in the range of 200–300 GPa.[34] The maximum modulus obtained for the extruded PE samples is 70 GPa, which is greater than the modulus of aluminum and twice the specific modulus of steel:

A. Birefringence

The birefringence of the extrudates was evaluated from

$$\Delta n_T = \lambda/\tau \tag{9}$$

where Δn_T is the total birefringence of the fiber, λ is the wavelength, and τ is the sample thickness required to retard light by one wavelength, i.e., $t = d/R$, where d is the fiber diameter and R is the retardance. Amorphous orientation, f_{am}, was estimated from birefringence by using the equation proposed by Stein[45]

$$\Delta n_T = \Delta n_c X_c + \Delta n_{am}(1 - X_c) + \Delta n_d + \Delta n_f \tag{10}$$

where

$$\Delta n_c = \Delta n_c^\circ f_c \tag{11}$$

$$\Delta n_{am} = \Delta n_{am}^\circ f_{am} \tag{12}$$

and Δn_c° and Δn_{am}° are the intrinsic birefringence of perfectly oriented orthorhombic crystalline and amorphous phases, respectively, Δn_f is the form birefringence, Δn_d is the distortion birefringence, and X_c is the crystalline volume fraction.

Birefringence is not detectable in the original or unoriented polyethylene in the extruder reservoir even after isothermal crystallization at 0.49 GPa. Figure 9 shows the birefringence of fibers obtained by solid-state extrusion. The birefringence rapidly increases from zero to a value of 0.059 which is equal to the birefringence of a polyethylene single crystal at a draw ratio of 15.[42] Above this draw ratio the birefringence approaches essentially a plateau value. For fibers extruded near their ambient melting point, the birefringence is 0.061, which is greater than that of a polyethylene single crystal having orthorhombic form. It appears that as the extrusion temperature is lowered from 130 to 60 °C, the average orientation of the fiber is as discussed in section E and may be expressed[46] by

$$\sin^2\theta = \frac{2}{3}\left(1 - \frac{\Delta n_T}{\Delta n_{max}}\right) \tag{13}$$

where θ is the average angle of the chain molecules in crystalline and noncrystalline units from the extrusion direction and equals zero for complete orientation. Δn_T is the total birefringence and Δn_{max} is the maximum birefringence obtained for the perfectly oriented phases.

Other workers have reported similar birefringence vs. draw ratio curves, but with important differences.[46–52] Nakayama and Kanetsuna[52] obtained a maximum birefringence of 0.05 with values apparently independent of the extrusion temperature over the range 20 to 110 °C. Birefringence would be expected to be dependent on whether extrusion is carried out above or below

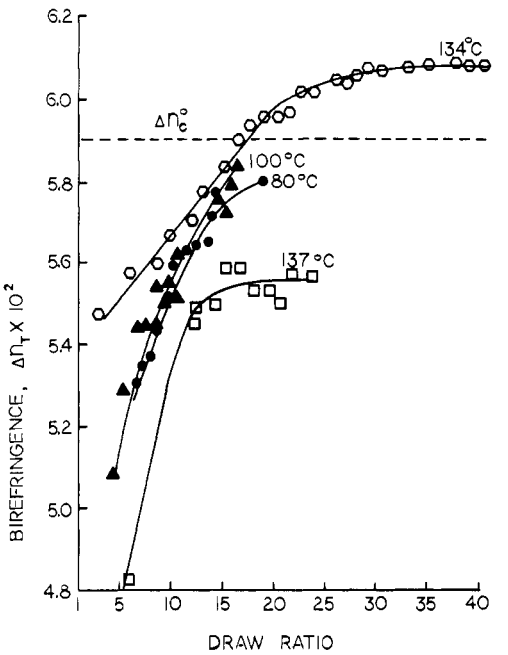

Figure 9. Birefringence vs. draw ratio of ultraoriented high-density polyethylene fibers extruded at 0.23 GPa and temperatures as shown.

the α-relaxation temperature range, as it is related to the relative contributions of the crystalline and noncrystalline contributions to the total birefringence. From the constant birefringence obtained in this laboratory at draw ratios of >15, it appears that the orientation of the fiber structure is essentially complete at these high draw ratios. Extrusion beyond draw ratios of 15 can only take place by displacement and/or further deformation of the fiber structure. The general form of the birefringence–draw ratio curves suggests that the general pattern of anisotropy of the ultraoriented fibers may be described by a model of rodlike crystallites in a noncrystalline matrix.[43] The crystalline axis rotates toward the extrusion direction. Such a model predicts for pseudoaffine deformation that the birefringence rapidly increases and approaches a maximum Δn_{max}, where

$$\Delta n_T = \frac{\Delta n_{max}}{2}\left[\frac{3}{1-k^2} - \frac{3k\cos^{-1}k}{(1-k^2)^{3/2}} - 1\right] \tag{14}$$

$k = \lambda^{-3/2}$ and λ is the extrusion or draw ratio. This is one of the few appropriate models available in the literature[47–51] that can be used to compare with experiment.

Comparison of the birefringence data in Figure 9 with extrusion rate data reported by Mead and Porter[10] suggests that the variation of extrusion rate with extrusion temperature may be responsible for the variation of the crystalline weight fraction of the fiber as well as the relative contributions and rate of orientation of the crystalline and noncrystalline phases. Figure 9 shows the birefringence of the HDPE fibers crystallized at 134 °C and 0.23 GPa and extruded at 80, 100, 134, and 137 °C.

A birefringence value of 0.062 ± 0.002 obtained for the HDPE fibers extruded near the ambient melting point is one of the highest values reported for HDPE. H. DeVries of Akzo Labs, Amsterdam, has independently measured the birefringence of these fibers. At an extrusion draw ratio of 36 a value of 0.0637 ± 0.0015 was observed. These birefringence values exceed the calculated value for the intrinsic birefringence of the crystalline phase, equal to 0.059.[45]

B. Wide-Angle X-ray Analysis

A diffraction pattern consisting of concentric rings of uniform intensity was obtained prior to extrusion of HDPE, indicating that

TABLE II. Orientation Functions and Partial Transformation from Orthorhombic to Monoclinic Phase

		monoclinic phase, equatorial intensity ratio				orthorhombic phase, orientation functions			
draw ratio	extrusion temp, °C	$f_{monoclinic}$[a]	I_{110}[b]	$I_{monoclinic}$[c]	intensity ratio	f_{110}	f_{200} (f_a)	f_b[d]	f_c
6.2	80		12.432	1.117	0.09				
15.4	80	−0.4356	6.026	0.786	0.13	−0.4275	−0.4435	−0.4208	0.8643
6.2	134		14.096	0.095	0.007	−0.4971	−0.4969	−0.4972	0.9941
40.3	134	−0.4939	21.456	1.530	0.07	−0.4965	−0.4957	−0.4968	0.9925

[a] Monoclinic lines at 4.55 Å (equatorial). [b] Background taken at $2\theta = 23.00°$, peak at 21.70°. [c] Background taken at $2\theta = 18.50°$, peak at 19.70°. [d] Calculated by using $f_b = -(f_a + f_c)$.

even after pressure has been applied for crystallization, the polyethylene is isotropic. After an extrusion at a draw ratio of 10–15, the X-ray intensity is confined to sharp azimuthal maxima indicative of high crystal orientation. The diffraction spots are indexed according to the orthorhombic cell spacings, and the patterns are discussed in detail by Desper et al.[53]

Table II shows the equatorial intensity ratios and orientation function of the monoclinic and orthorhombic reflections. The partial transformation from orthorhombic (O) to monoclinic (M+) phase is a characteristic result of cold working polyethylene.[54-59] The Bragg reflection angles (2θ) of about 19.4° and 23.0° correspond, according to Seto,[58] to the 001 and 200 reflections of the monoclinic phase. Lowering of extrusion temperature from 134 °C down to 80 °C produces a marked increase in the partial transformation from O to M structure as shown in Table II. The transformation also increases with draw ratio. The formation of monoclinic crystals gives some insight into the deformation process. Molecular segments that are in the amorphous phase or in chain folds will become aligned at high draw. with the highly aligned chains parellel to the fiber axis, the difference in energies between the two structures is governed by van der Waals forces. The thermodynamic stability of the orthorhombic form has been attributed to the lower vibrational free energy. Extrusion at higher pressure should also increase the partial transformation from O to M structure. The pressure also increases the yield stress, according to the Mohr criterion. The monoclinic phase may transform to the orthorhombic form on release of the pressure, so the values in Table II represent a lower bound to monoclinic formation during extrusion. Desper et al.[53] reported WAX analysis of fibers extruded at 136 °C and noted a faint line at $d = 4.56$ Å. This line was suggested to arise from a small amount of monoclinic structure, probably due to annealing during extrusion. Kiho et al.[55] detected a transformation from M to O above 100° due to stress relaxation. The stresses of the noncrystalline phase can relax by the instability of the needle-like and extended crystalline phase and/or by molecular migration relieving the retractive forces of the noncrystalline phase. The stress transformation in deformed PE has been discussed also be Rault.[60]

C. NMR Studies

The application of nuclear magnetic resonance (NMR) to the study of oriented polyethylene fibers has received considerable attention in the literature. Recently Ward has reviewed the measurement of molecular orientation in polymers by spectroscopic techniques.[43]

Figure 10 shows the derivative wide-line NMR signal for HDPE (Du Pont Alathon 7050, $M_w = 90\,000$) extruded at 120 °C and 0.23 GPa, using the method described by Capiati et al.[4] γ is the angle between the fiber axis and the steady magnetic field, H_0. The spectrum shows two components; the broader one is due to relatively rigid regions of the sample and the narrower component to nuclei whose motion is greater than 10^5 Hz. These components are associated with the crystalline and noncrystalline regions, respectively. With highly oriented polymers, the molecular motion is reduced, and it has been observed

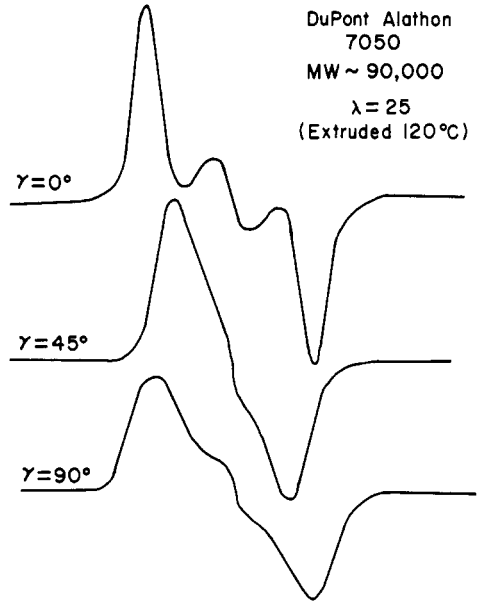

Figure 10. Derivative wide-line NMR spectra for HDPE (Du Pont Alathon 7050) extruded to draw ratio of 25 at 120 °C for three orientations with respect to the static magnetic field. γ = 0, 45, and 90° (after D. Presz, T. Stengle, and R. S. Stein[62]).

that the narrow component is reduced with orientation. Such observation is reasonable considering that the amorphous phase is also oriented during the deformation process. By varying the angle between the directions of orientation and magnetic field, it is possible to obtain information about the structure of the polymer. Using a method described by Bergman,[61] Presz et al.[62] determined the orientation of the two phases by calculating the second moment of each component.

Further NMR studies of the extruded HDPE fibers have been made by VanderHart[63] and Opella and Waugh.[64] VanderHart reported weak $^{13}C-^{13}C$ dipolar satellites in the spectra of the ultraoriented PE. The satellite splitting arising from the ith pair is

$$\Delta = 1.5\gamma_c^2 h^2 \frac{(1 - 3\cos^2\theta_i)}{R_i^3} \qquad (15)$$

where R_i is the distance between the ^{13}C nuclei, γ_c is nuclear gyroscopic ratio, and θ_i is the angle between R_i and H_0. Equation 15 is satisfied for polyethylene at 70 kHz field containing 1.1% natural-abundance ^{13}C. Figure 11 shows the carbon-13 cross-polarization spectrum of ultraoriented PE with a draw ratio of 11.8. The R_1 pair of satellites corresponding to directly bonded ^{13}C nuclei was resolved, but for the R_2 and R_3 satellites corresponding to ^{13}C pairs two and three bonds away, only the high-field component was visible; the low-field satellites overlapped with the spectra arising from unoriented chains. A different approach to the NMR studies of the highly oriented fibers was reported by Opella and Waugh. The NMR procedure of separated local-field spectroscopy was used to complement the NMR study of VanderHart.

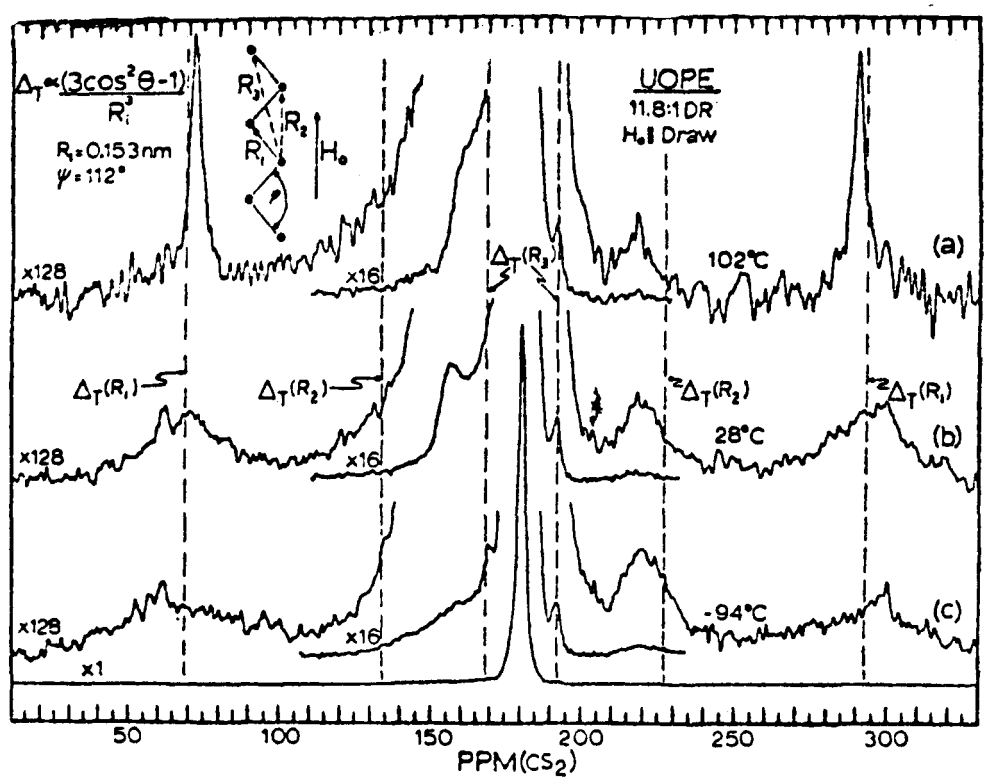

Figure 11. Carbon-13 cross-polarization spectra of ultraoriented linear polyethylene with draw ratio of 11.8. The draw direction is parallel to the magnetic field. The three pairs of $^{13}C-^{13}C$ dipolar satellite positions based on $R_1 = 0.153$ nm and $\psi = 112°$ are given by the dashed lines (after D. L. Vanderhart[63]).

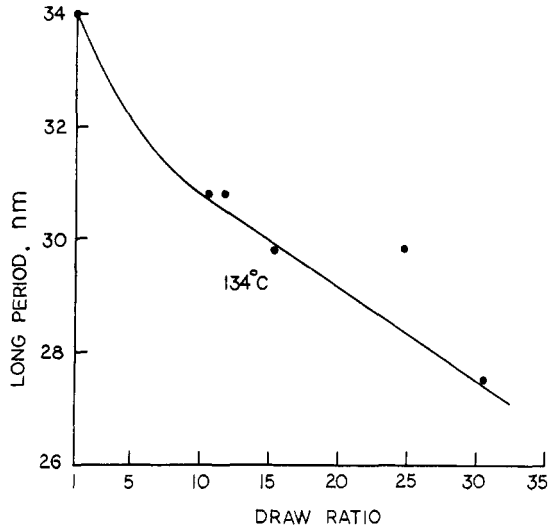

Figure 12. Long-period dependence on draw ratio of the ultraoriented high-density polyethylene extruded at 0.23 GPa and 134 °C.

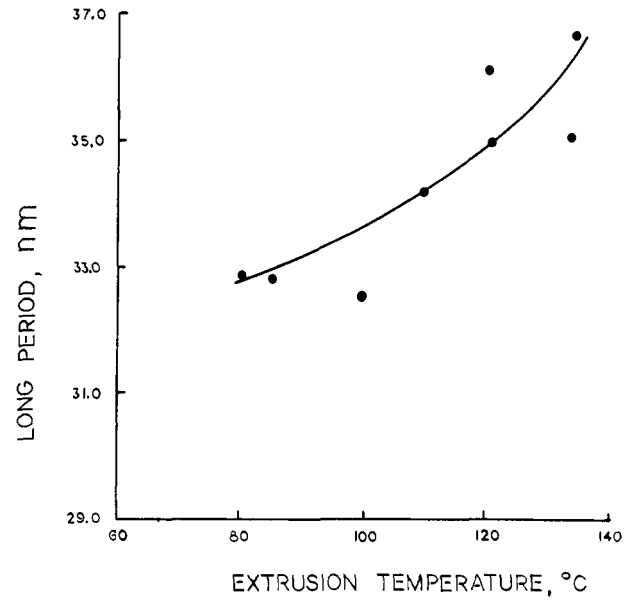

Figure 13. Axial long period, calculated from the maxima of small-angle X-ray scattering, of ultraoriented fibers, vs. extrusion temperature.

D. Small-Angle X-ray Measurements

The intensity of the first-order diffraction in the small-angle region of X-ray scattering with a regular stacking of lamellae is given by

$$I_n \propto (\rho_c - \rho_{am})^2 \sin^2 \frac{\pi t}{L} \qquad (16)$$

where L is the periodicity of lamellar stacking, t is the thickness of the interlamellar noncrystalline zone, and ρ_c and ρ_{am} are the electron densities of the corresponding phases. The long period is calculated from the scattering maximum according to Bragg's law.

Figure 12 shows the long-period variation with draw ratio for a fiber extruded at 134 °C and 0.23 GPa. The effect of extrusion temperature on the long period of fibers with draw ratio of 10 is shown in Figure 13. The photographs show a two-point pattern for all fibers reported herein, i.e., intensity maxima on the meridian of the diffraction pattern which is parallel to the fiber axis. At extrusion draw ratios <5, maxima are observed perpendicular to the fiber axis and are possibly associated with voiding. Within the error of the measurement (estimated to be ±20 Å), there is probably an increase of long period with extrusion temperature and a small decrease, ~50 Å, with extrusion draw ratio. Similar observations have been reported by Imada et al., Nakayanama and Kanetsuna, and Farrell and Keller.[7,52,39] The effect of extrusion pressure on the long periods is negligible. The long periods of the fibers are thus primarily determined by

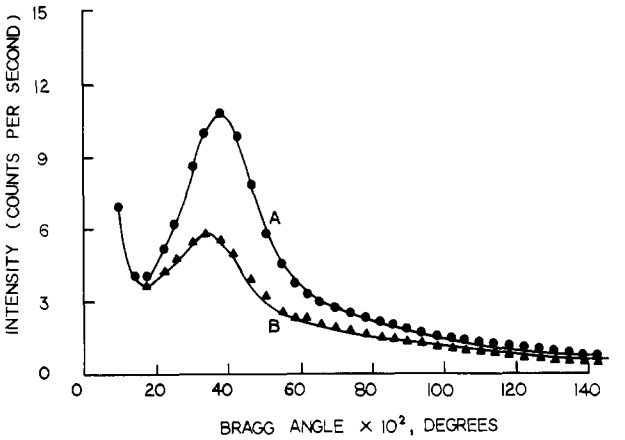

Figure 14. Intensity variation vs. Bragg angle plot at draw ratios of (A) 5 and (B) 40 for an extruded high-density polyethylene fiber. Extrusion temperature and pressure were 134 °C and 0.23 GPa.

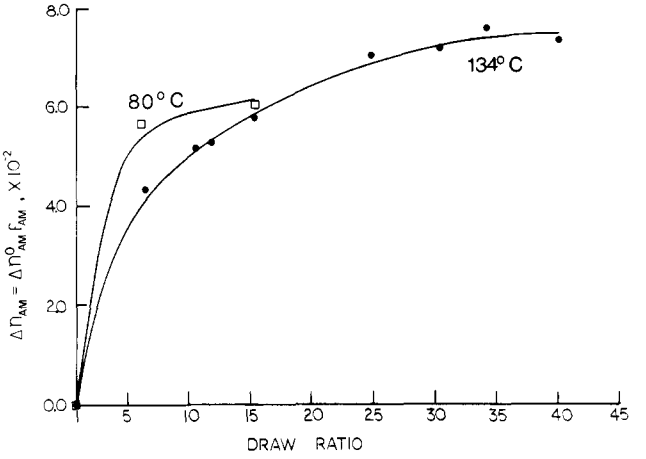

Figure 15. Variation of Δn_{am} with draw ratio for ultraoriented high-density polyethylene extruded at 0.23 GPa and temperatures as shown.

the extrusion draw ratio and extrusion temperature. The variation of the long period with temperature and pressure indicates, as pointed out by Peterlin,[65] partial chain refolding. Chain folds and the orientation of lamellae perpendicular to the extrusion direction will lower fiber modulus. Of course, polyethylene which has not undergone deformation exhibits a SAXS pattern having uniform and isotropic intensity distribution. Fiber extrusion immediately produces two intensity maxima, as described, indicating that the crystal surfaces in the conical die region and fiber are becoming more highly oriented in planes perpendicular to the extrusion axis.

Figure 14 shows the SAXS curves or $I_{obsd}(2\theta)$ obtained using a Kratky camera. The scattering intensity decreases but does not vanish with extrusion draw ratio. A decrease in the intensity of the scattering of a strong meridional peak obtained from highly drawn polyacetal fibers was also reported by Clark and coworkers.[35,66] The areas of $I_{obsd}(2\theta)$ under the maxima are in the ratio of 3:1 for extruded fibers having draw ratios of 5 and 40. These areas should correlate with the tensile modulus and may be used as a measure of fiber perfection since the absence of long-period scattering is indicative of chain folds in low concentration and/or folds distributed throughout the fibril as defects in a continuous noncrystalline and/or crystalline matrix.

E. Degree of Orientation

The amorphous orientation function, f_{am}, was estimated from eq 10 with Δn_d and Δn_f set to zero. The variation of $\Delta n_{am} = \Delta n_{am}{}^{\circ} f_{am}$ with draw ratio is shown in Figure 15 for extrusion at 80 and 134 °C. The product $\Delta n_{am}{}^{\circ} f_{am}$ increases rapidly with

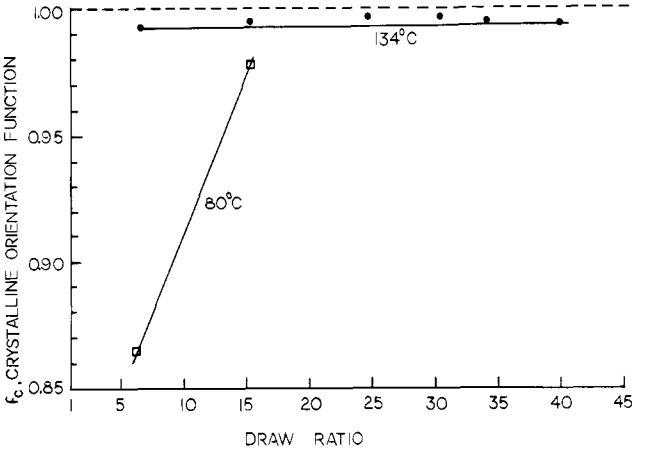

Figure 16. Variation of crystalline orientation function, f_c, with draw ratio for ultraoriented high-density polyethylene extruded at 0.23 GPa and temperatures as shown.

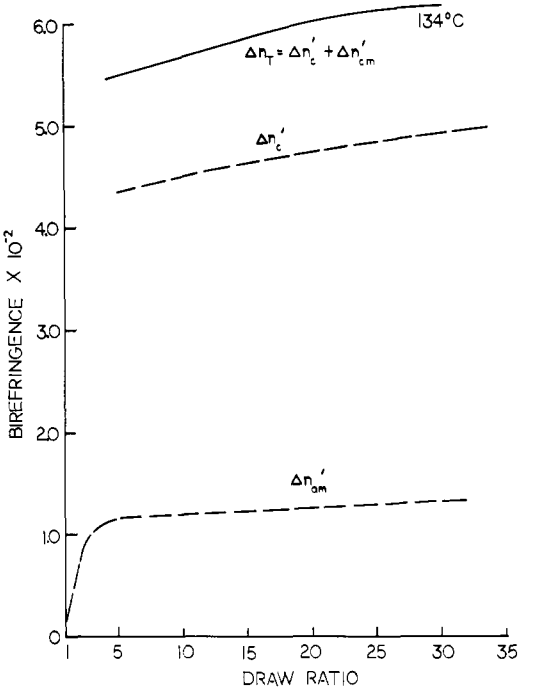

Figure 17. Noncrystalline and crystalline birefringence contributions of high-density polyethylene extrudate.

draw ratio and approaches a constant value of 0.075. At lower extrusion temperatures, the noncrystalline orientation markedly increases. This is in agreement with Nakayama and Kanetsuna,[52] who found that amorphous orientation increased as the hydrostatic extrusion temperature was decreased from 110 to 20 °C. For deduction of the amorphous orientation function, the intrinsic birefringence of amorphous polyethylene is required.

Denbigh[67] and other workers[68-71] report values in the range 0.2–0.3 for the intrinsic birefringence of the noncrystalline phase of polyethylene. On the basis of values reported in the literature for the intrinsic birefringence, the maximum amorphous orientation function for fibers extruded at 134 °C should be ~0.3.

Figure 16 shows the crystal orientation as a function of draw ratio for extrusions at 80 and 134 °C. The wide-angle X-ray photographs of fibers at all draw ratios exhibit typical *c*-axis diffraction patterns. At 134 °C f_c at draw ratios from 5 to 40 is 0.994 ± 0.002 and independent of draw ratio and extrusion rate.

Mead et al.[72] characterized the *a*- and *b*-axis orientation by azimuthal scannings of the 200 and 110 reflections. At low draw ratio the orientation of the *a* axis of the fiber extruded at 80 °C

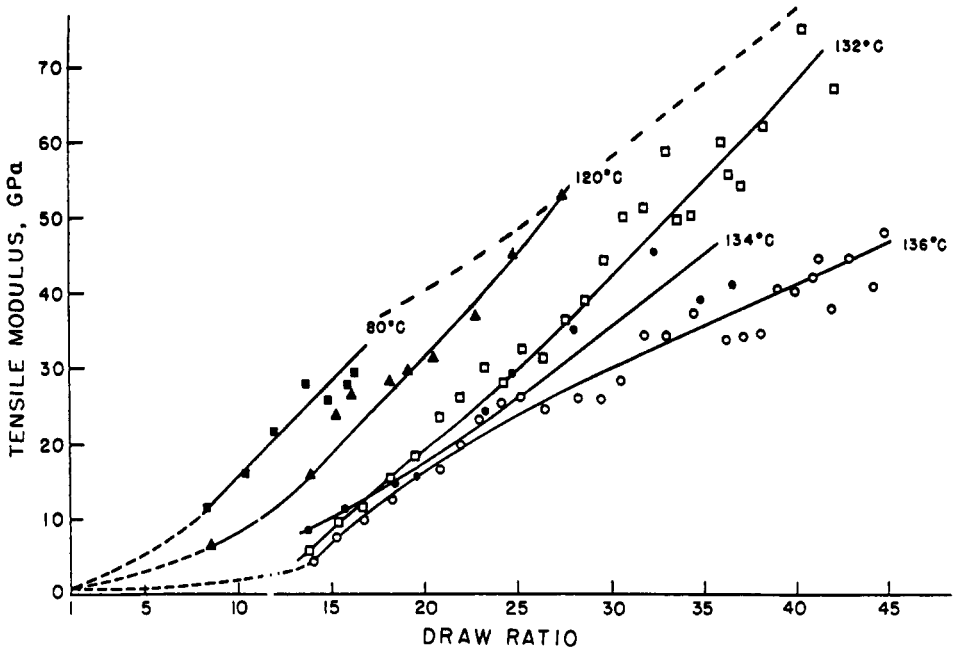

Figure 18. Dependence of tensile modulus of fiber draw ratio at various extrusion temperatures. The high-density polyethylene was crystallized at 0.23 GPa and 134 °C.

tends to align perpendicular to the fiber axis and orients more readily than the *b* axis.[73] This is consistent with the results of the low-temperature hydrostatic extrusion experiments of Nakayama and Kanetsuna.[52]

Stein[74-76] has shown that the birefringence per unit volume of crystalline material is

$$\Delta n_c = f_a(n_a - n_c) + f_b(n_b - n_c) \quad (17)$$

where f_a, f_b are the crystalline orientation functions along the *a* and *b* axes and n_a, n_b, and n_c are the refractive indices parallel to the respective axes. Subtraction of the crystalline contribution from the total fiber birefringence results in the noncrystalline contribution, as shown in Figure 17. The birefringence of HDPE fiber extruded at 134 °C is determined by the high crystalline contribution, arising from the almost perfect *c*-axis orientation and crystallinity. The noncrystalline contribution approaches a maximum at high draw ratio and accounts for the maximum birefringence being greater than $\Delta n_c°$.

F. Mechanical Measurements

Tensile Modulus

At draw ratios less than 10–15 the modulus slowly increases with draw ratio, as the spherulitic morphology is deformed in the conical die. At draw ratios over 10–15 the modulus increases rapidly and linearly with draw ratio up to the maximum obtainable, prior to fiber fracture. Figure 18 shows a plot of the tensile modulus of the fibers as a function of draw ratio over the range 80–136 °C prepared at 0.23-GPa extrusion pressure. The modulus increase appears to occur by two different mechanisms, as indicated by the two different shapes of the tensile modulus curves. The modulus rapidly increases, corresponding to that draw ratio where strain hardening occurs; this is indicated by the rapid increase in apparent elongational viscosity.[10] This particular draw ratio also corresponds with the onset of a negative expansion coefficient of the fiber, a limit of crystallinity, melting point, amorphous and crystalline orientation, and birefringence. As shown by Halpin and Kardos,[77] the modulus should approach an upper limit

$$E_{11} = E_f V_f + E_m V_m \quad (18)$$

TABLE III. Tensile Strength Measurements of Extruded High Density Polyethylene

extrusion temp, °C	draw ratio variation	tensile strength, GPa	ref
134	5–15	0.24	72
	15–25	0.38	
	25–35	0.41	
120	5–15	0.30	
	15–20	0.25	
80	5–15	0.35	
134	30–40	0.4	82

The maximum modulus obtained at each extrusion temperature is limited by fracture. The dotted line in Figure 18 is the fracture envelope of modulus vs. draw ratio where fracture is first observed. Importantly, the modulus–draw ratio curves do not show a plateau with increasing draw ratio, unlike the highly drawn polyoxymethylene fibers of Clark and Scott.[35] The form of the curves is very similar to that obtained by Barham and Keller[78] and Capaccio et al.[79] for drawn single crystals and drawn HDPE. The modulus variation with extrusion temperature when compared at a given extrusion pressure and draw ratio apparently show that the most efficient way to produce high modulus fibers is to extrude at a temperature near the α-relaxation temperature range. According to Capaccio and Ward,[79] the modulus variation is a unique function of draw ratio. Peterlin[65] considers the extrusion of crystalline polymers at high pressure and below the melting point to be similar to the process of conventional drawing under tension. The enhanced properties of the solid-state extrudate compared to the drawn material are due to the better lateral fit of the fibrillar elements and the better compaction of the structural defects at the microfibril ends due to compressive stresses. Hence high-pressure extrusion produces a fiber with increasing density.

The effet of external pressure on the elastic modulus has been discussed by Sauer et al.[80] Nonlinear elasticity theory must be used to account for the high stresses obtained at high pressure. According to the equation given by Birch,[81] the relationship between modulus and pressure is a function only of Poisson's ratio. Poisson's ratio for the ultraoriented fibers may be expected to be less than 0.5 for the oriented fibers, so that the increasing pressure should increase the modulus of the fiber.

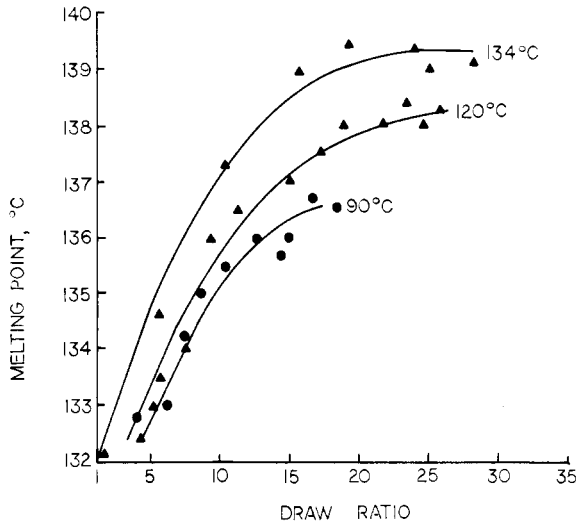

Figure 19. Dependence of endotherm peak melting point with draw ratio of ultraoriented HDPE fibers extruded at 0.23 GPa and temperatures as shown.

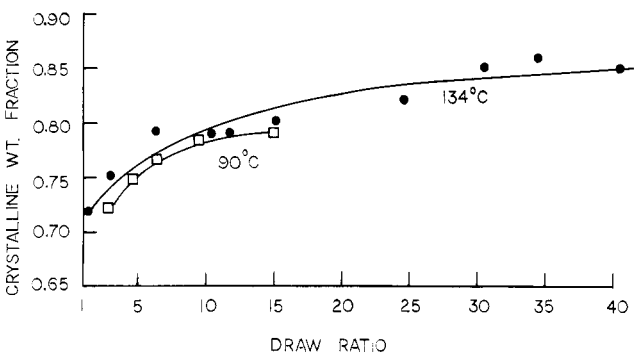

Figure 20. Crystalline weight fraction vs. draw ratio of high-density polyethylene extruded at 0.23 GPa.

Tensile Strength

As shown in Table III, tensile strength approaches a limit with increasing draw ratio. A maximum value of 0.4 GPa reported by Porter and co-workers[72,82] has been obtained over a draw ratio of ~10–15.

Kojima, Desper, and Porter[83] studied the influence of draw ratio and extrusion temperature on tensile strength and found that the latter approaches a limit at high draw ratios, independent of extrusion temperature over the range 134–110 °C. A small increase in tensile strength was found by decreasing the temperature from 134 to 80 °C. Recently, extrusion of higher molecular weight polyethylene in the range of 110–120 °C produced ultraoriented polyethylene fibers with tensile strength values as high as 0.6 GPa.[84]

G. Thermal Analysis

Figures 19–22 show the melting point and crystalline weight fraction for HDPE fibers extruded at the temperatures shown and at pressures of 0.23 and 0.49 GPa. For extrusion at 134 °C the peak melting point and crystallinity, X_c, of the fiber extruded at 0.23 GPa increase to a maximum of ~139 °C and 0.85 (heating rate of 10 °C min^{-1}), as the result of ultraorientation. However, lowering of the extrusion temperature decreases both the resultant X_c and the melting point because extrusion at lower temperature does not produce the most perfect crystal morphology.

Thermomechanical analysis (TMS) data for ultraoriented fibers have been reported[85] in terms of either an average linear expansion coefficient, $\alpha_{av} = (1/L_{20})\Delta L/\Delta T$, where L_{20} is the length of the fiber at room temperature (20 °C), or the coefficients of linear expansion α and of volumetric thermal expansion β. These coefficients are defined as

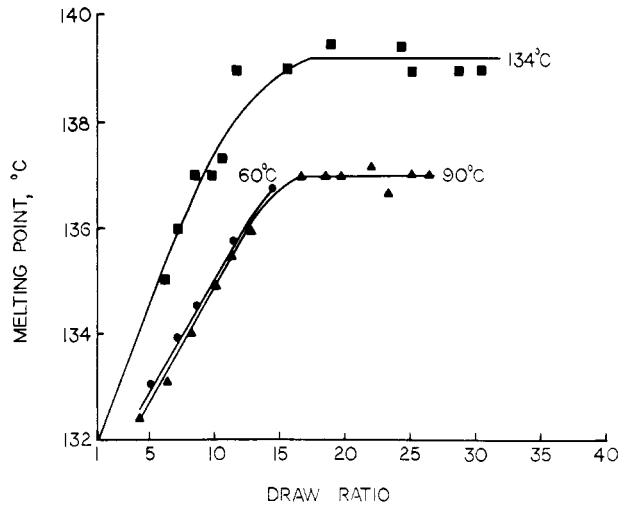

Figure 21. Dependence of endotherm peak melting point with draw ratio of ultraoriented high-density polyethylene fibers extruded at 0.49 GPa and temperatures as shown.

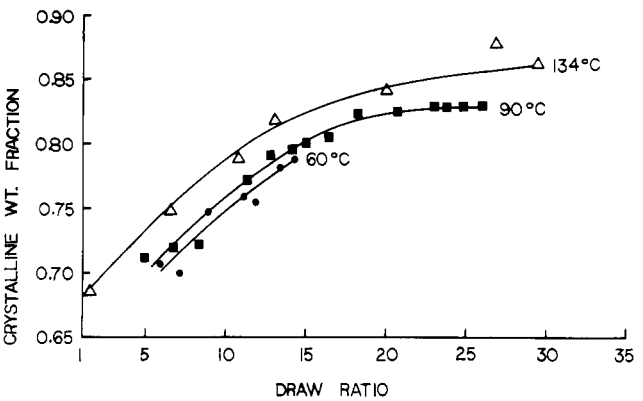

Figure 22. Crystalline weight fraction vs. draw ratio of high-density polyethylene extruded at 0.49 GPa and temperatures as shown.

$$\alpha = \frac{1}{L_T}\frac{dL_T}{dT} \tag{19}$$

and

$$\beta = \frac{1}{V_T}\frac{dV_T}{dT} \tag{20}$$

ΔL and ΔV are the changes in length and volume of the fiber and L_T and V_T are length and volume at T °C.

The dimensional changes of the fibers are a function of draw ratio, as shown in Figures 23 and 24. At a draw ratio of unity, α_{11} is positive and comparable to that for an unoriented HDPE (~3×10^{-4} °C^{-1}). At a higher draw ratio, α_{11} becomes negative; the change of α_{11} from positive to negative corresponds to the two stages of deformation described by Mead and Porter.[10] The average linear expression coefficients of the ultraoriented fibers at high draw ratio follow approximately the thermal expansion of the crystallographic axes. Davis et al.[86] report that $\alpha_a = 3.1 \times 10^{-4}$ °C^{-1}, $\alpha_b = 0.7 \times 10^{-4}$ °C^{-1}, and $\alpha_c = -12 \times 10^{-6}$ °C^{-1} at room temperature. Values of the average expansion coefficient perpendicular to the fiber axis were found to be independent of draw ratio and equal to ~3×10^{-4} °C^{-1}.

The negative expansion coefficient has been cited as evidence for the fibers containing a component of chain-extended morphology[76] with planar zigzag packing in an orthorhombic unit

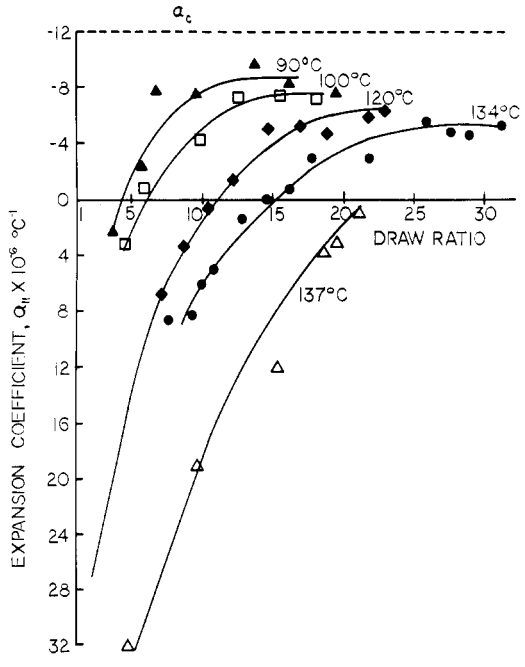

Figure 23. Variation of linear expansion coefficient with draw ratio of ultraoriented high-density polyethylene fibers extruded at 0.23 GPa and temperatures as shown.

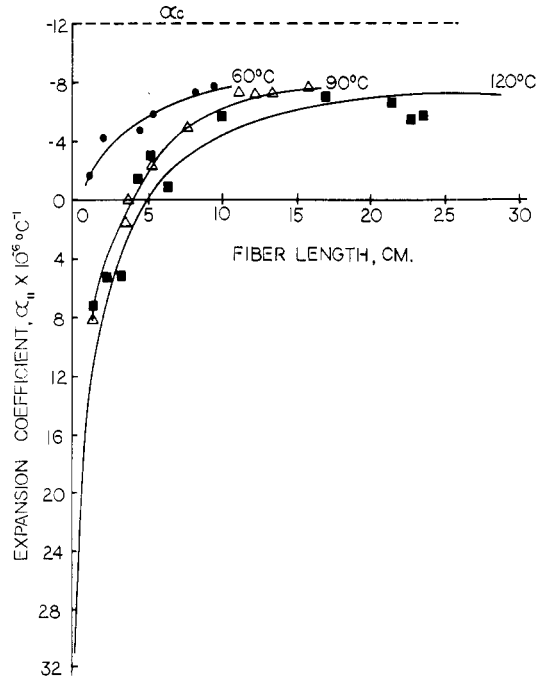

Figure 24. Variation of linear expansion coefficient with draw ratio of ultraoriented high-density polyethylene fibers extruded at 0.49 GPa and temperatures as shown.

cell. The contraction along the chain axis of -12×10^{-6} °C^{-1} corresponds to a 2° average twist due to limited chain rotation from trans to gauche.[87] The variation of α_{11} with temperature illustrated in Figures 24 and 25 has been shown to be consistent with the thermal instability associated with the anisotropy of the crystal surface free energies in the ultraoriented crystalline fibers as well as other sources of melting point reduction such as defects.[88] Such a model for the annealing characteristics observed is consistent with the results of Desper et al.,[53] who showed that the amorphous phase is essentially randomly oriented for polyethylene extruded near the ambient melting point of 132 °C. However, the noncrystalline orientation increases as the extrusion temperature is lowered. The marked shrinkage behavior, and hence creep behavior, of the extruded fibers at temperatures above 20 °C are possible due to the relaxation of the strained molecular chains in the amorphous phase. Hence the relatively high values of the expansion coefficient of the fiber extruded at 90 °C, shown in Figures 22 and 23, do not indicate that a more perfect crystal is being extruded. This is further demonstrated in Figures 19–22 by the drop in melting point and crystallinity on lowering extrusion temperature. The increased shrinkage is more likely to result from the restoring forces of the stressed amorphous phase. Hence analysis of the annealing behavior of ultraoriented polyethylene reported by Mead and Porter[88] can only apply for fibers extruded near the ambient melting point, where the amorphous phase is essentially of random orientation.[53] Their analysis cannot be valid at the lower extrusion temperatures, nor can the model of a continuous crystalline phase be applicable if the degree of crystallinity and orientation decrease on lowering the extrusion temperature. The model proposed by Peterlin, as described above, seems more appropriate. However, at extreme orientation, the fully extended tie moleule and crystallites may not be distinguished as separate phases.

Finally, a summary of physical properties of ultraoriented high-density polyethylene fibers is given in Table IV. The values are compared with those for a single crystal.

V. Deformation Structures and Fracture

Deformation mechanisms similar to those in polymer crystals must be expected when ultraoriented fibers attain properties similar to those of crystals. The ultraoriented fibers have a high longitudinal modulus, ~70 GPa, but must have transverse tensile and shear moduli at least an order of magnitude lower because of only van der Waals bonding between adjacent chains.

Kolbeck and Uhlmann[89] and Shigematsu et al.[90] have discussed the formation of oblique deformation structures (kink bands) during compression testing of solid-state extruded fibers. They did not note that similar deformation bands and fracture can be obtained during solid-state extrusion at the highest draw ratios. Kink bands are often formed as a result of deformation of oriented crystalline polymers. The deformation mechanisms in extruded fibers at high draw ratios appear to be similar to the kink band formation reported by Shigematsu et al.[90] and produced by compressive deformation of oriented extrudates. The first visible indication of the deformation bands in drawn fibers is the whitening associated with the generation of voids within the deformation bands. In extruded fibers oblique fracture planes are observed. Shigematsu accounted for the formation of the deformation structures by two mechanisms: *c*-axis slip of the microfibrils and shear of the lamellar crystallites by slip parallel to the *c*-axis direction. Kolbeck and Uhlmann[89] proposed a third mechanism involving interlamellar slip to account for the deformation band formation structures.

The fracture envelope or deformation band formation as a function of extrusion temperature is shown in Figure 18. The maximum modulus for each fiber is plotted against draw ratio, onset of the deformation bands producing a drop in modulus. Comparison of these data with the noncrystalline orientation results shown in Figure 13 indicates that when fracture is first observed the amorphous orientation functions at 80 and 134 °C are at a maximum and have similar values. These observations give support to the interlamellar slip mechanism proposed by Kolbeck and Uhlmann.[89]

Lowering of the extrusion temperature rapidly reduces the fiber extrusion rate. The deformation bands also occur more readily at lower draw ratios as the extrusion temperature is decreased. The formation of the deformation bands does not appear to be related to fiber strain rate. At lower extrusion temperatures the degree of crystallinity and crystalline orientation decreases so that slip in the chain direction may not be possible, resulting thus in fracture of the noncrystalline phase.

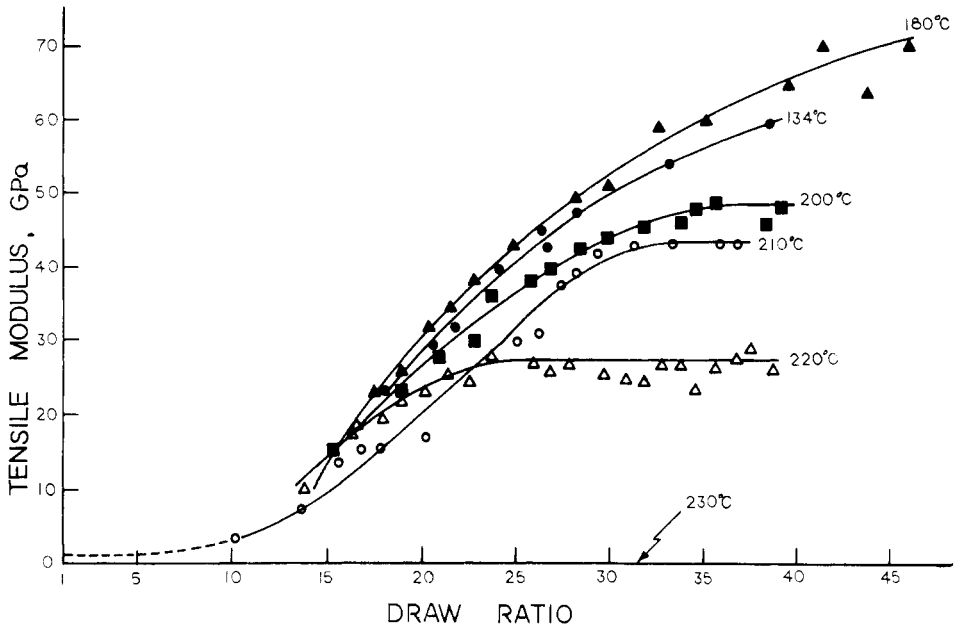

Figure 25. Dependence of tensile modulus on fiber draw ratio at various crystallization temperatures. The high-density polyethylene was crystallized at 0.49 GPa and extruded at 120 °C and 0.49 GPa.

TABLE IV. Comparison of Physical Properties of UMass Ultraoriented HDPE Fibers (in the Chain Direction) with Single-Crystal Characteristics

physical property	polyethylene single crystal (ref)	properties of UMass ultradrawn high-density polyethylene fibers
modulus, GPa	285, 240 (34, 94)	70
tensile strength, GPa	13 (95)	0.4
strain to fracture, %	6 (95)	3, $M_w = 60\,000$
minimum and maximum obtainable draw ratio prior to fracture	calculated minimum draw ratio required to fully extend chains (35) = 86 for $M_w = 10^4$ 86 for $M_w = 10^6$	extrusion at 60 °C, $M_w = 60 \times 10^3$, maximum obtainable draw ratio of 13.8 extrusion at 134 °C, $M_w = 147 \times 10^3$, maximum obtainable draw ratio = 40
linear expansion coefficient, 10^{-5} °C^{-1}	*a* axis + 22 (86) *b* axis + 3.8 *c* axis −1.2	−0.9 ± 0.1, fiber axis
melting point, °C	145.5 °C (15)	139 °C (10 °C min^{-1} DSC scan rate)
crystalline fraction	crystallinity density (40), 1.008 g cm^{-3}	0.85 extrusion of chain-folded PE
	amorphous density 0.855 g cm^{-3}	0.95 extrusion of chain-extended PE
crystal orientation function	1.000	0.996 ± 0.002
birefringence total	$\eta_a = 1.514$ (53) $\eta_b = 1.519$ $\eta_c = 1.575$ $\Delta\eta_c = 0.059$	0.0618 ± 0.002[a]

[a] A value of 0.0637 ± 0.0015 was obtained by Dr. H. DeVries using the same fiber.

The onset of fracture or formation of the deformation structures can be deduced from the form of the apparent elongational viscosity curves as a function of true strain. At lower extrusion temperatures, η_E rapidly increases and approaches values comparable to a glass. When $d\eta_E/d \ln [DR(r)]$ rapidly increases and η_E approaches 10^{12} Pa·s, then the stresses at the conical wall are sufficient to exceed the critical shear stress for interlamellar or interfibrillar slip. Chain slip in PE takes place at a constant critical resolved shear stress of 15 ± 1 MPa.[91]

The deformed structures more readily occur at lower extrusion temperatures, suggesting that the deformation bands are associated with deformation of the amorphous phase. Bowden and Young[92] showed that the elastic part of the deformation of HDPE with a well-defined lamellar crystal morphology can be accounted for by interlamellar slip.

Polymer crystals can deform plastically by twinning, by slip, and by a stress-induced martensitic phase transformation. The latter mechanism of orthorhombic to monoclinic phase transformation has been shown to occur.[54-59] At the highest draw ratios the deformation bands proliferate, and deformation of the ultraoriented fiber is not expected to take place without also destroying the crystalline order. For temperatures ≥132 °C the fibers are also annealed on extrusion and the crystallinity decreases. Concomitant with fracture is the accelerated increase of the extrusion rate as shown by the length vs. time characteristic which deviates from the extrapolated length–time variation of the steady state. This total length difference should give the total length change due to slip along the fiber direction. Such a marked deviation in extrusion rate, particularly near 132 °C, would indicate that plastic deformation is proceeding by slip since large plastic deformations can only be obtained by this mechanism. Indeed Bowden and Young[92] and Krause and Yeh[93] have suggested that it is the ease of[100] [001] slip at elevated temperatures which allows HDPE to be highly strained and attain high modulus. Fracture of the small fraction of amorphous phase would also result in loss of the drawing mechanism. This is further demonstrated by the extrusion of various initial morphologies of polyethylene through a conical die under constant extrusion temperature and pressure conditions.[11] Figure 25 shows the tensile modulus vs. draw ratio of extruded high-density polyethylene crystallized at 0.49 GPa and various temperature, as shown, cooled to 120 °C and extruded at 0.49 GPa. Brittle fracture occurs when crystallinity approaches 100% and when chain-extended lamellae of micron dimensions are produced at the high pressure and a crystallization temperature near 230 °C.

VI. Concluding Remarks

In this article we discussed the solid-state extrusion process in terms of the extrusion conditions, extrusion variables, and their

effects on the physical and mechanical properties of high-density polyethylene extrudates. By selecting the processing conditions we can produce effectively high draw ratios and markedly enhance the mechanical performance of high-density polyethylene drastically.

Acknowledgments. We express appreciation to the Engineering Division of the National Science Foundation for support of this study.

VII. References

(1) J. H. Southern and R. S. Porter, *J. Macromol. Sci., Phys.*, **B4**, 541 (1970).
(2) J. H. Southern and R. S. Porter, *J. Appl. Polym. Sci.*, **14**, 2305 (1970).
(3) J. H. Southern, N. E. Weeks, and R. S. Porter, *Makromol. Chem.*, **102**, 19 (1972).
(4) N. J. Capiati, S. Kojima, W. G. Perkins, and R. S. Porter, *J. Mater. Sci.*, **13**, 334 (1977).
(5) B. Wunderlich and T. Arakawa, *J. Polym. Sci., Part A*, **2**, 3697 (1964).
(6) R. S. Porter, J. H. Southern, and N. E. Weeks, *Polym. Eng. Sci.*, **15**, 213 (1975).
(7) K. Imada and M. Takayanagi, *Int. J. Polym. Mater.*, **2**, 71 (1973); **2**, 89 (1973).
(8) K. Imada, T. Yamamoto, K. Shigematsu, and M. Takayanagi, *J. Mater. Sci.*, **6**, 537 (1971).
(9) S. Maruyama, K. Imada, and M. Takayanagi, *Int. J. Polym. Mater.*, **2**, 125 (1973); *ibid* **1**, 211 (1972).
(10) W. T. Mead and R. S. Porter, *J. Polym. Sci., Polym. Symp.*, in press (accepted 1977).
(11) W. T. Mead and R. S. Porter, Flow Induced Crystallization Symposium, Midland Macromolecular Institute, Midland, MI, Aug 1977.
(12) J. M. Alexander, *Mater. Sci. Eng.*, **10**, 70 (1972).
(13) P. D. Griswold, A. E. Zachariades, and R. S. Porter, Flow Induced Crystallization Symposium, Midland Macromolecular Institute, Midland, MI, Aug 1977.
(14) T. Shimada, A. E. Zachariades, M. P. C. Watts, and R. S. Porter, *Polym. Prepr. Am. Chem. Soc., Div. Polymn. Chem.*, **20**, 2 (1979).
(15) A. Peterlin, *J. Polym. Sci., Part C*, **9**, 61 (1965).
(16) A. G. Gibson, I. M. Ward, B. N. Cole, and B. N. Parsons, *J. Mater. Sci.*, **9**, 1193 (1974).
(17) I. L. Hay and A. Keller, *Kolloid-Z.-Polym.*, **204**, 43 (1965).
(18) H. D. Keith and F. J. Padden, *J. Polym. Sci.*, **41**, 525 (1969).
(19) K. Sasaguri, S. Hoshino, and R. S. Stein, *J. Appl. Phys.*, **35**, 47 (1964).
(20) R. S. Stein, S. Onogi, K. Sasaguri, and D. A. Keedy, *J. Appl. Phys.*, **34**, 80 (1963).
(21) Y. F. Yu and K. Ullman, *J. Polym. Sci.*, **60**, 55 (1962).
(22) P. Ingram and A. Peterlin, *J. Polym. Sci., Part B-2*, 739 (1964).
(23) R. S. Stein, *Acc. Chem. Res.*, **5**, 121 (1972).
(24) R. Yang and R. S. Stein, *J. Polym. Sci., Part A-2*, **5**, 939 (1967).
(25) D. N. Bigg, *Polym. Eng. Sci.*, **16**, 725 (1976).
(26) A. Peterlin, *J. Mater. Sci.*, **6**, 490 (1971).
(27) A. Peterlin, *Text. Res. J.*, **42**, 20 (1972).
(28) A. Peterlin, *Annu. Rev. Mater. Sci.*, **2**, 349 (1972).
(29) J. Becht, K. L. DeVries, and H. H. Kausch, *Eur. Polym. J.*, **7**, 105 (1971).
(30) J. Becht and H. Fisher, *Kolloid-Z.-Polym.*, **240**, 766 (1970).
(31) R. S. Porter, *Polym. Prepr., Am. Chem. Soc.*, **12**, No. 2 (1971).
(32) J. M. Andrews and I. M. Ward, *J. Mater. Sci.*, **5**, 411 (1970).
(33) T. L. Smith, *Polym. Eng. Sci.*, **13**, 161 (1973).
(34) F. C. Frank, Proc. *R. Soc. London, Ser. A*, **319**, 127 (1970).
(35) E. S. Clark and L. S. Scott, *Polym. Eng. Sci.*, **14**, 682 (1974).
(36) G. R. Snelling and J. F. Lontz, *J. Appl. Polym. Sci.*, **3**, 257 (1960).
(37) J. W. Hill and J. A. Cuculo, *J. Appl. Polym. Sci.*, **18**, 2569 (1974).
(38) H. Eyring, *J. Chem. Phys.*, **4**, 283 (1936).
(39) C. J. Farrell and A. Keller, *J. Mater. Sci.*, **12**, 966 (1977).
(40) L. A. Davis and C. A. Pampillo, *J. Appl. Phys.*, **42**, 4659 (1971).
(41) J. D. Hoffman, G. Williams, and E. Passaglia, *J. Polym. Sci., Ser. C*, **14**, 173 (1966).
(42) I. M. Ward, *Proc. Phys. Soc., London*, **80**, 1176 (1962).
(43) I. M. Ward, *J. Polym. Sci.*, **58**, 1 (1977).
(44) P. J. Miller, J. F. Jackson, and R. S. Porter, *J. Polym. Sci.*, **11**, 2001 (1973).
(45) R. S. Stein, *J. Polym. Sci.*, **31**, 327 (1958).
(46) D. Patterson and I. M. Ward, *Trans. Faraday Soc.*, **53**, 1516 (1957).
(47) W. Kuhn and F. Grun, *Kolloid-Z.*, **101**, 248 (1942).
(48) H. Kolsky and A. C. Shearman, *Proc. R. Soc. London, Ser. B*, **62**, 111 (1949).
(49) S. M. Crawford and H. Kolsky, *Proc. Phys. Soc. London, Sect. B*, **64**, 119 (1951).
(50) T. Williams, *J. Mater. Sci.*, **8**, 59 (1973).
(51) I. M. Ward, *Proc. Phys. Soc.*, **80**, 1176 (1959).
(52) K. Nakayama and H. Kanetsuna, *J. Mater. Sci.*, **10**, 1105 (1975).
(53) C. R. Desper, J. H. Southern, R. D. Ulrich, and R. S. Porter, *J. Appl. Phys.*, **41**, 4284 (1970).
(54) F. C. Frank, A. Keller, and A. O'Connor, *Philos. Mag.*, **3**, 64 (1958).
(55) H. Kiho, A. Peterlin, and P. H. Geil, *J. Polym. Sci., Part B*, 157 (1965).
(56) D. Krueger and G. S. Y. Yeh, *J. Appl. Phys.*, **43**, 4339 (1972).
(57) A. Turner Jones, *J. Polym. Sci.*, **62**, 53 (1962).
(58) T. Seto, T. Hara, and K. Tanaka, *Jpn. J. Appl. Phys.*, **7**, 31 (1968).
(59) K. Tanaka, T. Seto, and T. Hara, *J. Phys. Soc. Jpn.* **17**, 873 (1962).
(60) J. Rault, *J. Macromol. Sci., Phys.*, **B12**, 335 (1976).
(61) K. Bergmann, *Kolloid-Z. Z. Polym.*, **251**, 961 (1973).
(62) D. Presz, T. Stengle, and R. S. Stein, to be published.
(63) D. L. VanderHart, *J. Magn. Reson.*, **24**, 467 (1976).
(64) S. J. Opella and J. S. Waugh, *J. Chem. Phys.*, **66**, 4919 (1977).
(65) A. Peterlin, *Polym. Eng. Sci.*, **16**, 127 (1976).
(66) W. N. Taylor and E. S. Clark, *Polym. Prepr., Am. Chem. Soc., Div. Polym. Chem.*, **18**, 332 (1977).
(67) K. G. Denbigh, *Trans. Faraday Soc.*, **36**, 936 (1940).
(68) S. D. Hong, C. Chang, and R. S. Stein, *J. Polym. Sci.*, **13**, 1447 (1975).
(69) Y. Fukui, T. Asada, and S. Onogi, *Polym. J.*, **3**, 100 (1972).
(70) A. N. Gent and V. V. Vickroy, *J. Polym. Sci., Part A-2*, **5**, 47 (1967).
(71) D. W. Saunders, D. R. Lightfoot, and D. A. Parsons, *J. Polym. Sci., Part A-2*, **6**, 1183 (1968).
(72) W. T. Mead, C. R. Desper, and R. S. Porter, to be published.
(73) R. S. Stein, *J. Polym. Sci.*, **34**, 709 (1959).
(74) R. S. Stein, *J. Polym. Sci., Part A-2*, **7**, 1021 (1959).
(75) R. S. Stein, *J. Polym. Sci.*, **32**, 335 (1950).
(76) R. S. Stein and F. H. Norris, *J. Polym. Sci.*, **21**, 381 (1956).
(77) J. C. Halpin and J. L. Kardos, *J. Appl. Phys.*, **43**, 2235 (1972).
(78) P. J. Barham and A. Keller, *J. Mater. Sci.*, **11**, 27 (1976).
(79) G. Capaccio, T. A. Compton, and I. M. Ward, *J. Polym. Sci., Part A-2*, 164 (1976).
(80) J. A. Sauer, K. D. Pae, and S. K. Bhateja, *J. Macromol. Sci., Phys.*, **B8**, 631 (1973).
(81) F. Birch, *J. Appl. Phys.*, **9**, 4 (1938).
(82) N. J. Capiati and R. S. Porter, *J. Polym. Sci.*, **13**, 1177 (1975).
(83) S. Kojima, C. R. Desper, and R. S. Porter, *J. Polym. Sci., Polym. Phys. Ed.*, in press (accepted 1977).
(84) T. Kanamoto, A. E. Zachariades, and R. S. Porter, *J. Polym. Sci., Polym. Phys. Ed.*, **17**, 2171 (1979).
(85) R. S. Porter, N. E. Weeks, N. J. Capiati, and R. J. Krzewki, *J. Therm. Anal.*, **8**, 547 (1975).
(86) G. T. Davis, R. K. Eby, and J. P. Colson, *J. Appl. Phys.*, **41**, 4316 (1970).
(87) R. H. Baughman and E. A. Turi, *J. Polym. Sci.*, **11**, 2453 (1973).
(88) W. T. Mead and R. S. Porter, *J. Appl. Phys.*, **47**, 4278 (1976).
(89) A. G. Kolbeck and D. R. Uhlmann, *J. Polym. Sci., Part A-2*, **15**, 27 (1976).
(90) K. Shigematsu, K. Imada, and M. Takayanagi, *J. Polym. Sci., Part A-2*, **13**, 73 (1975).
(91) P. B. Bowden and R. J. Young, *J. Mater. Sci.*, 2034 (1974).
(92) P. B. Bowden and R. J. Young, *Nature (London), Phys. Sci.*, **229** (1), 23 (1971).
(93) S. J. Krause and G. S. Y. Yeh, *Bull. Am. Phys. Soc.*, **CH8**, **22**, 312 (1977).
(94) J. Sakurada, T. Ito, and K. Nakamae, *J. Polym. Sci., Part C*, **15**, 75 (1966).
(95) A. Peterlin, *Polym. Eng. Sci.*, **9**, 172 (1969).